Current Biology 19, 287–296, February 24, 2009 ©2009 Elsevier Ltd All rights reserved DOI 10.1016/j.cub.2009.01.055

Article

# Spindle Fusion Requires Dynein-Mediated Sliding of Oppositely Oriented Microtubules

Jesse C. Gatlin,[1,2,*] Alexandre Matov,[4] Aaron C. Groen,[1,3] Daniel J. Needleman,[1,3] Thomas J. Maresca,[1,2] Gaudenz Danuser,[4] Timothy J. Mitchison,[1,3] and E.D. Salmon[1,2]

[1]Cell Division Group
Marine Biological Laboratory
Woods Hole, MA 02543
USA

[2]Department of Biology
University of North Carolina at Chapel Hill
Chapel Hill, NC 27599
USA

[3]Department of Systems Biology
Harvard Medical School
Boston, MA 02115
USA

[4]Department of Cell Biology
Laboratory for Computational Cell Biology
The Scripps Research Institute
La Jolla, CA 92037
USA

## Summary

**Background: Bipolar spindle assembly is critical for achieving accurate segregation of chromosomes. In the absence of centrosomes, meiotic spindles achieve bipolarity by a combination of chromosome-initiated microtubule nucleation and stabilization and motor-driven organization of microtubules. Once assembled, the spindle structure is maintained on a relatively long time scale despite the high turnover of the microtubules that comprise it. To study the underlying mechanisms responsible for spindle assembly and steady-state maintenance, we used microneedle manipulation of preassembled spindles in *Xenopus* egg extracts.**

**Results: When two meiotic spindles were brought close enough together, they interacted, creating an interconnected microtubule structure with supernumerary poles. Without exception, the perturbed system eventually reestablished bipolarity, forming a single spindle of normal shape and size. Bipolar spindle fusion was blocked when cytoplasmic dynein function was perturbed, suggesting a critical role for the motor in this process. The fusion of Eg5-inhibited monopoles also required dynein function but only occurred if the initial interpolar separation was less than twice the microtubule radius of a typical monopole.**

**Conclusions: Our experiments uniquely illustrate the architectural plasticity of the spindle and reveal a robust ability of the system to attain a bipolar morphology. We hypothesize that a major mechanism driving spindle fusion is dynein-mediated sliding of oppositely oriented microtubules, a novel function for the motor, and posit that this same mechanism might also be involved in normal spindle assembly and homeostasis.**

*Correspondence: jgatlin@email.unc.edu

## Introduction

Establishing and maintaining a bipolar steady state in microtubule assembly dynamics is critical for chromosome segregation. During spindle assembly, microtubules are nucleated from centrosomal and noncentrosomal sources, requiring cells to integrate microtubules nucleated at multiple, spatially distinct sites into a single bipolar array [1, 2]. Interestingly, if groups of chromosomes are initially far enough apart at entry into mitosis or are physically separated from one another, they each can form bipolar spindles that are capable of fusing into a single metaphase spindle [3, 4]. In this case, achieving bipolarity in the final metaphase spindle requires adjacent spindles to align all chromosomes onto a single equatorial plate and to reduce the total number of poles to two. Similar microtubule-dependent mechanisms may also be important for chromosome alignment within an individual bipolar spindle because kinetochores can initiate microtubule formation and elongation independently of the spindle pole [5–7].

The fusion of two preassembled spindles is likely controlled by the same fundamental mechanisms that govern normal spindle assembly and steady-state maintenance. In acentrosomal female animal meiosis, spindle assembly results from motor-dependent organization of microtubules nucleated and stabilized around chromatin [1]. Two microtubule motors in particular, Kinesin 5 (Eg5) and cytoplasmic dynein-dynactin (dynein), make important mechanistic contributions. Eg5 is a homotetrameric motor that crosslinks and slides oppositely oriented microtubules apart where they overlap at the spindle midzone [8, 9]. This activity drives microtubule minus ends poleward and contributes substantially to microtubule poleward flux [10–12]. In contrast to Eg5, the minus end-directed motor complex dynein contains multiple microtubule-binding domains that likely bind to the same microtubule [13]. Thus, the dynein complex must form multimeric complexes or associate with other proteins in order to crosslink and slide microtubules.

In *Xenopus* egg extract spindles, dynein antagonizes Eg5 in regulating spindle morphology and length. Strong inhibition of Eg5 by the small molecule inhibitor monastrol causes the collapse of metaphase spindles into radial, monopolar microtubule arrays [14, 15], whereas perturbation of dynein function results in the splaying of spindle poles and, depending on the means of inhibition, spindle elongation [15–17]. Consistent with opposing functions, inhibiting both motors results in bipolar spindles of nearly normal length and shape that are structurally very fragile [15]. Recently proposed "slide and cluster" models posit that new microtubules are continuously formed near chromosomes in meiotic spindles (presumably by a RanGTP-regulated pathway [18]) and moved with their minus ends leading toward one or the other pole by Eg5 sliding [19]. As a result, microtubule minus ends are distributed throughout the spindle [20]. It is thought that these ends may be the attachment sites that dynein uses to oppose Eg5-mediated poleward microtubule sliding, but exactly how and where dynein acts to antagonize Eg5 are not known.

We reasoned that, by studying the interaction of two preassembled spindles, we may gain new insight into the mechanistic basis of microtubule motor function within the

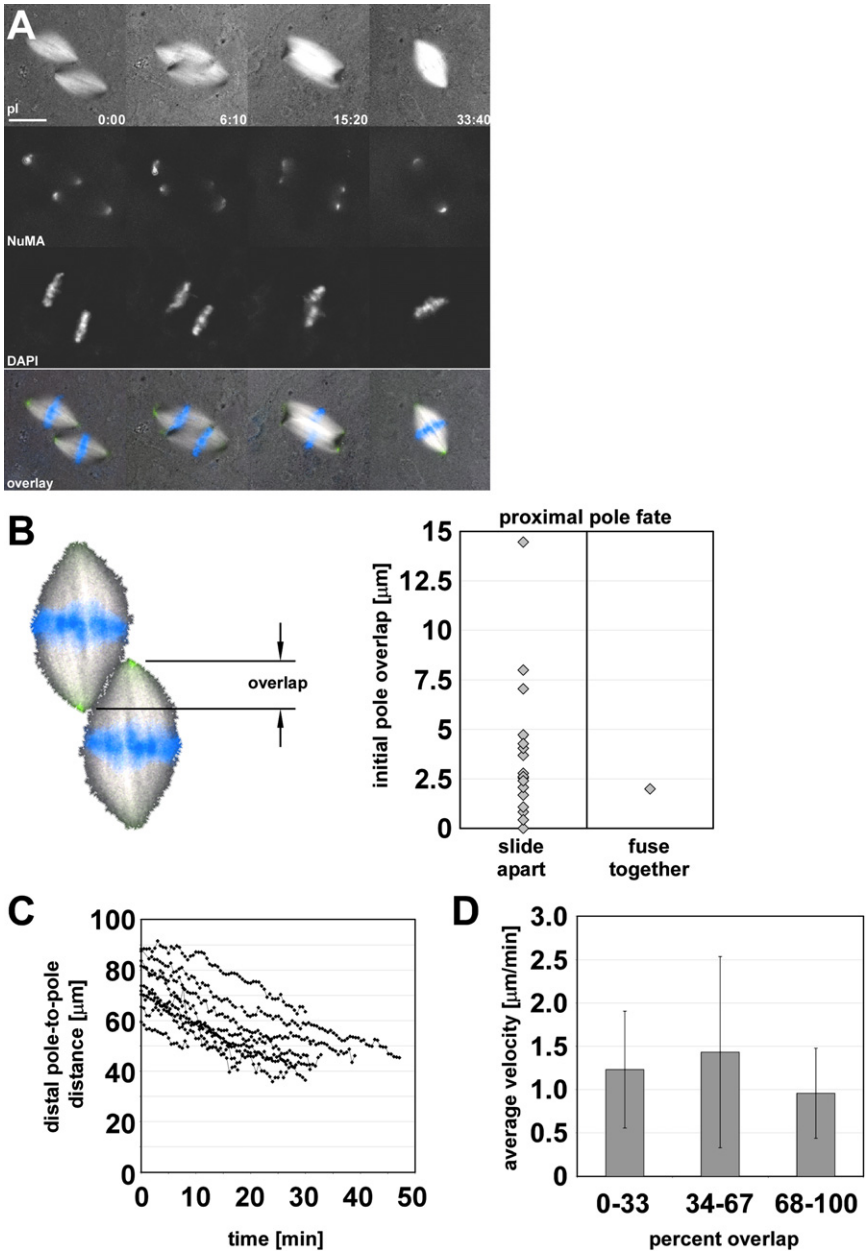


Figure 1. Parallel Spindles with Overlapped Poles Merge by Sliding

Meiosis II arrested bipolar spindles were positioned by using microneedles with their interpolar axes parallel and with overlapped proximal poles. Subsequent alignment and fusion was monitored with polarization optics and fluorescence microscopy (A). Directly labeled anti-NuMA antibodies were added to the extracts to mark the poles, and DAPI was used to label the chromosomes at the metaphase plate. In this starting configuration, the majority of spindles fused by sliding parallel to the interpolar axis (A and B). In (C), the position of the distal poles is plotted versus time. For all time courses, the zero time point represents the time that the first image was acquired following spindle positioning. This typically occurred within a few seconds after moving the microneedles away from the spindles. The average velocity of alignment (the slope) is 1.2 ± 0.4 μm/min (n = 9 spindle pairs). For (D), the same data as in (C) were used to determine the velocity as a function of percent overlap (i.e., 100 × overlap/average initial spindle length). Values were obtained by averaging the slopes of linear regressions for sliding that occurred during the fraction of overlap indicated. Analysis with a pairwise Student's t test indicated no statistically significant differences between the velocities (all $p > 0.05$). Scale bars represent 25 μm.

spindle. We found that bipolar spindles will indeed fuse if brought close enough together with microneedles and do so in distinct ways depending on their initial spatial arrangement. Fusion also occurred between closely opposed pairs of Eg5-inhibited monopoles. In both cases, fusion depended on dynein function. Based on these observations and additional analyses of microtubule dynamics during fusion, we propose a model in which dynein generates pulling forces between poles by sliding microtubules of opposite polarity. Our results suggest a novel function for the dynein motor that has implications for meiotic spindle morphogenesis and length regulation.

## Results

### Nearby Spindle Pairs Align and Fuse with Each Other

We first tested how two spindles interacted if their axes were parallel to each other and their ends overlapped as shown in Figure 1 (see also Movies S1 and S2 available online). Once two spindles were manipulated to touch each other and held there for ~30 s or more, they adhered strongly and became impossible to pull apart by micromanipulation without distortion of both spindles. In this parallel orientation, the spindles indeed fused and did so by sliding where the proximal, overlapped poles moved apart, increasing the length of the overlap until the spindles eventually aligned pole to pole (Figures 1A and 1B). During parallel spindle sliding, antiparallel microtubule overlap between adjacent spindles is expected to be maximal when the spindles are half-overlapped with a pole of each spindle aligned with the equator of the other. As the spindles slide further together, the amount of antiparallel overlap should decrease. Assuming that the motors responsible for spindle fusion rely on a specific orientation of interacting microtubules (e.g., Eg5 or dynein), one might expect sliding velocity to vary as a function of overlap. The average velocity of sliding was determined from the slopes of linear regressions of the plots shown in Figure 1C and found to be 1.2 ± 0.4 μm/min (n = 9 spindle pairs, minimum $R^2 = 0.91$). This value did not vary significantly as the amount of overlap changed (Figure 1D).

Spindle poles, decorated with fluorescently labeled antibodies against NuMA, remained largely intact during spindle alignment by sliding, whereas chromosomes, visualized with DAPI, demonstrated persistent alignment on the equator of each spindle during sliding. Lateral movements of poles and chromosomes completed fusion of the two spindles into one, a process that usually occurred more slowly than sliding

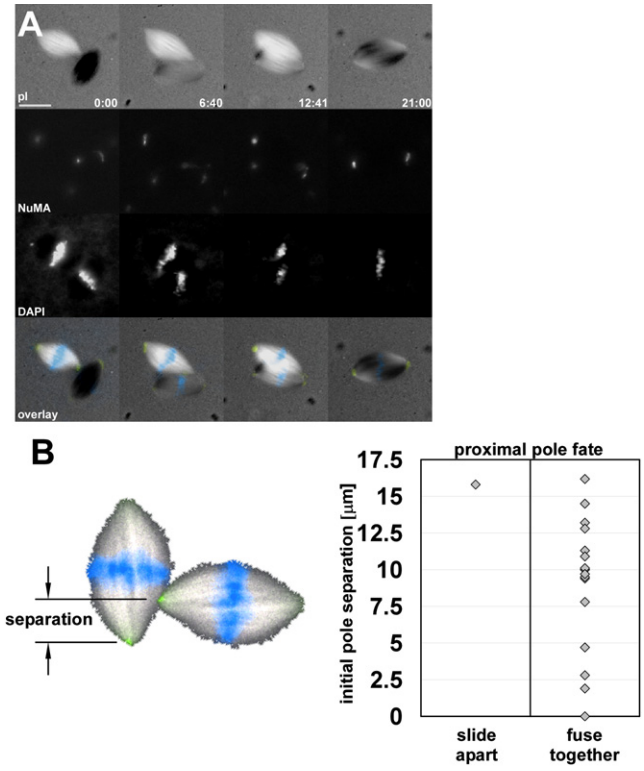


Figure 2. Perpendicular Spindles Merge by "Jackknifing"

Spindles positioned with perpendicular interpolar axes were monitored as in Figure 1. "T-boned" spindles also align, but, in the absence of antiparallel microtubule overlap, the proximal poles come together as the spindles rotate, ultimately creating a single, fusiform bipole (A and B). The graph in (B) shows the fate of the proximal poles plotted by the initial spacing between them. In almost all cases, the two nearest poles moved together and fused. Scale bars represent 25 μm.

alignment of the metaphase plates (Figure 1A). Following spindle fusion, the resultant microtubule array was always a bipolar spindle. On average, these spindles were ~10% longer than the initial two spindles (Figure S1A; [21]). Interestingly, the microtubule content of the resulting steady-state structures, as measured by integrated fluorescence intensity of spindle-incorporated labeled tubulin, was approximately half of the total content from the sum of its two predecessors (Figure S1B).

We then tested whether antiparallel spindle microtubule interactions were required for efficient fusion of two adjacent spindles. This was done by placing one spindle axis orthogonal to the other ("T-bone" geometry) (Figures 2A and 2B and Movie S3). In this geometry, initial movement of the proximal poles toward each other was coupled to a rotation of one or both spindles, which brought their axes closer to parallel (with one exception; n = 17 spindle pairs). The two spindles then slid into alignment, similar to spindles positioned in parallel with pole overlap as in Figure 1. We refer to the rotational component of spindle alignment as "jackknifing."

### Pulling Forces on Peripheral Spindle Microtubules Contribute to Spindle Fusion

Spindle jackknifing suggests the existence of traction forces between poles. We reasoned that these forces were the result of motor-mediated sliding of interacting microtubules extending from each pole. Although not evident by using low-power objectives, higher-resolution confocal imaging of fluorescently labeled tubulin (Figure 3A) or EB1 (Figure 3B and Movie S4) revealed a low density of peripheral microtubules that radiate outwards from the spindle poles at all angles to the spindle axis. To test whether these microtubules could pull poles together and to estimate their distance of action, we positioned spindles end to end with their interpolar axes aligned and their proximal poles separated by various distances (Figure 3D and schematic in 3E). The critical distance for interaction in this geometry was ~10 microns; spindles this far apart or closer typically interacted and moved to bring their proximal poles together, whereas spindles further apart typically did not (Figure 3E). In eight out of ten cases, the proximal poles fused, and then one or both spindles pivoted around the now shared pole and jackknifed to form a single bipolar spindle (Figure 3D). In two out of ten cases, the proximal poles moved together but then continued to slide past each other, aligning by the sliding mode shown in Figure 1. Spindles positioned side by side with various separation distances and orientations of their interpolar axes also fused when sufficiently close (the two closest poles within ~35 μm) (Figure S2). We suspect that the critical interaction distance depends on spindle orientation because peripheral microtubules are longer extending from the pole outward away from the sides of the spindle compared to extending away from the back of the pole (Figures 3A–3C).

### Bipolar Spindle Alignment and Fusion Require Cytoplasmic Dynein

Pole-focusing mechanisms are typically mediated by minus end-directed motors. In *Xenopus* egg extracts, there are two prominent motors with this directional polarity: cytoplasmic dynein and XCTK2, a member of the kinesin-14 family of motors [22]. To investigate the possible role of either motor in spindle fusion, we first treated fully assembled bipolar spindles with 25 μM $Na_3VO_4$ (vanadate) prior to micromanipulation and asked what effect this would have on bipolar fusion. This vanadate concentration has been shown to inhibit cytoplasmic dynein motor activity with no measureable effect on that of XCTK2 [23]. As expected for dynein inhibition, vanadate caused spindle widening and an increase in spindle length that occurred at a rate of ~5 um/min, the rate that overlapping microtubules slid apart within the spindle (by fluorescent speckle microscopy; data not shown) [16, 19]. This concentration of vanadate completely inhibited alignment and fusion of parallel, overlapped spindles (n = 11 spindle pairs) (Figure 4A and Movie S5). Unlike controls, in many instances, two spindles that were pushed and held together for ~30 s simply drifted apart when the microneedles were removed, suggesting that the formation of adhesive linkages between the two spindles was either slowed or did not occur altogether.

To rule out nonspecific effects of vanadate, we used two alternative approaches to inhibit dynein function. In the first, monoclonal antibody against the 70.1 kDa dynein intermediate chain (ab70.1) was added to extract containing fully assembled spindles. As previously shown [24], ab70.1 caused bipolar spindles to lose focus at the poles, elongate, and ultimately transform into barrel-shaped microtubule arrays with aligned chromosomes at their midpoint (Figure 4B and Movie S6). Similarly to vanadate-treated spindles, when these microtubule arrays were juxtaposed with no discernible space between the structures, they failed to adhere, align, and fuse (n = 8 spindle pairs) (Figure 4B). Spindle assembly following dynein immunodepletion from the extract (>97%, as

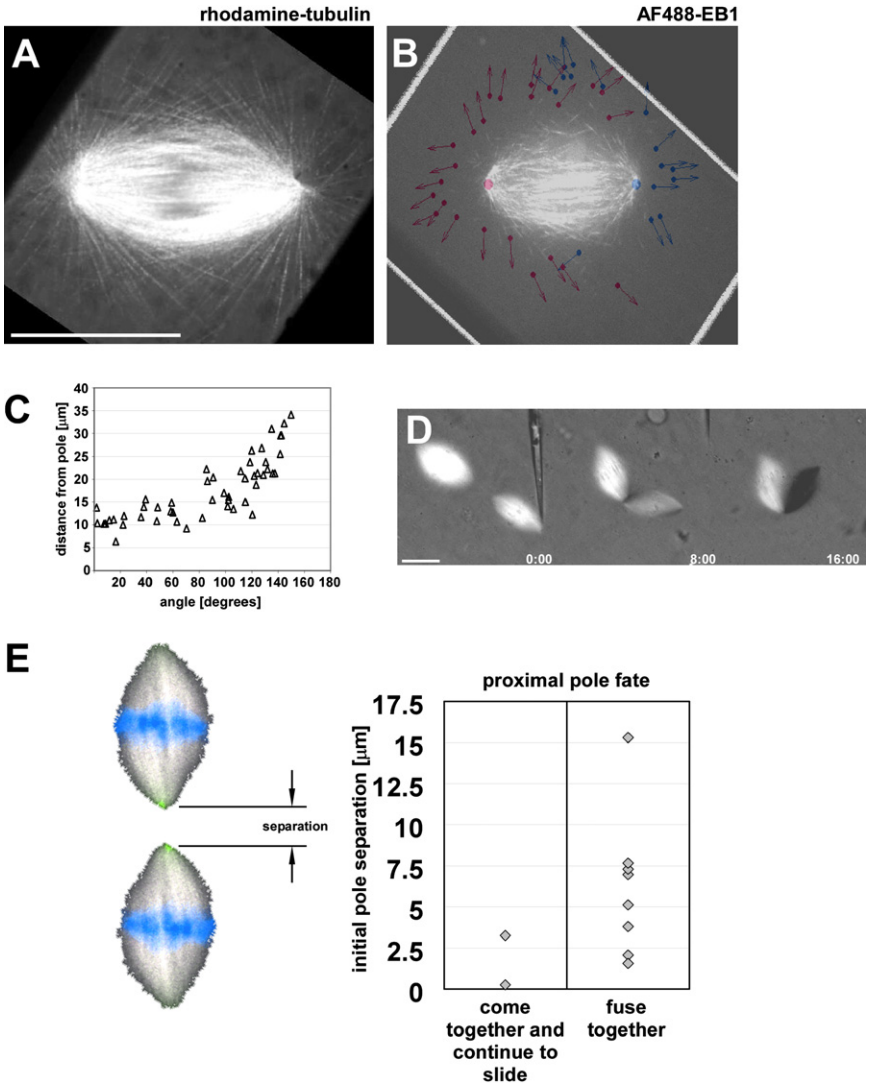


Figure 3. Peripheral Microtubules Facilitate Spindle Alignment and Fusion through a Distance

(A) High-resolution confocal imaging of rhodamine-tubulin-labeled spindles reveals numerous peripheral microtubules extending beyond the circumference of the main spindle body.

(B and C) Complementary studies with fluorescently labeled EB-1 (125 nM) added to preassembled spindles to visualize the dynamics of growing microtubule ends also show peripheral microtubules extending beyond the margins of the spindle. The image shown in (B) represents a single frame from a time-lapse series spanning ~2 min (result is typical of the n = 20 spindles observed). The centers of overlayed circles mark the most distal positions of EB1 trajectories observed during imaging, whereas the arrows indicate the direction of EB1 comet trajectories. Colors indicate from which pole the growing microtubule likely emanated from. This was determined by assuming a linear trajectory for each EB1 comet and finding the point where it intersected a line running through both spindle poles (i.e., the extended interpolar axis). The pole closest to this point was assumed to be from where the comet originated. In some cases, the comet trajectories did not intersect with the extended interpolar axis, so we simply assumed the comet originated from the nearest pole. The distances from the poles to each EB1 comet were plotted against the angle of the comet trajectory to the horizontal, with 0° oriented on the horizontal extending behind the pole and 180° on the horizontal toward the metaphase plate (C).

(D and E) To test whether spindles could merge through a distance, spindle pairs were positioned on the same axis with separation between their proximal poles (D). In most cases, the spindles first came together, fused at their proximal poles, and then pivoted or "jackknifed" around the shared pole (D and E). Scale bars represent 25 μm.

determined by western blot) (Figure S3) resulted in similar barrel-shaped spindles and had the same inhibitory effect on fusion (n = 9 spindle pairs) (Figure 4C and Movie S7). In contrast, in extracts depleted of the minus end-directed motor XCTK2, a condition that still allows for relatively normal bipolar spindle assembly [22], spindle-spindle adhesion and sliding were unaffected (n = 6 spindle pairs from 2 different extracts) (Figures 4D and S3 and Movie S8), although, qualitatively, pole fusion seemed to occur more slowly.

### Dynein Slides Overlapping Microtubules of Opposite Polarity

To further examine the role of dynein in spindle fusion, we assembled monopolar asters by inhibiting Eg5 with small molecule inhibitors that block ADP release and mimic loss of function of the motor (monastrol and the more potent drug S-trityl-L-cysteine [STLC]) [10, 25]. When two such monopoles were brought sufficiently close together by manipulation, they interacted, moved together at rates of 2.8 ± 0.8 um/min, and fused into a single monopole (for velocity measurements, n = 8 monopole pairs; the total number of monopole fusion observations was > 20) (Figure 5A and Movie S9). As they merged together, we often observed an increase in birefringence between the two poles that had a spindle-like shape, but the formation of this central spindle was variable in its occurrence, as shown in Figure 5A. The maximum initial interpolar separation that permitted merging was ~60 μm (Figure 5C, control). Analysis of monopole size, as measured by tracking growing plus ends with fluorescent EB1, revealed a marked decrease in the number of plus ends extending beyond a radius of 35 μm (Figure 5D), suggesting that overlap of plus ends is necessary to facilitate fusion. Interestingly, only one plus end (out of 1396 tracked) was found beyond 55 μm from the monopole center. Therefore, it is unlikely that long microtubules spanning from one monopole center to the other are required for fusion, although we cannot rule out the possibility that, during fusion, antiparallel overlap stabilizes microtubule dynamics, thereby generating some tubules that extend beyond this distance. Similar to bipoles, monopole fusion was completely inhibited by 25 μM vanadate (n = 9 monopole pairs) (Figures 5B and 5C and Movie S10). Importantly, this treatment did not appreciably change monopole size (i.e., diameter; data not shown), and overlap of microtubules near the edges of monopoles was evident provided that the initial separation distance was < ~60 μm. Alternative methods to inhibit dynein, like those employed in our bipole fusion experiments, proved

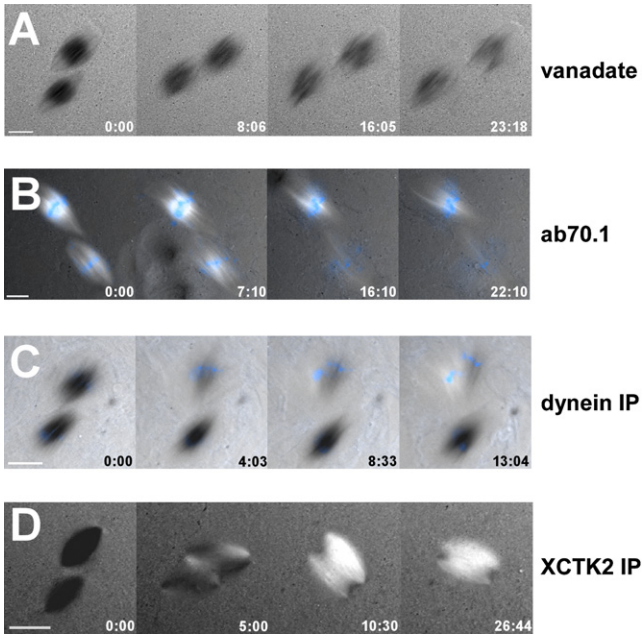


Figure 4. Dynein Is Required for Bipolar Spindle Alignment and Fusion

Polarization images of spindle pairs positioned with their proximal poles overlapped and their interpolar axes parallel to one another.

(A) Images of bipolar fusion from a time-lapse series following addition of 25 μM vanadate.

(B) Antibodies to dynein intermediate chain (final concentration ~1.0 mgml$^{-1}$) were added 5–10 min prior to the start of imaging. Notice that spindle alignment and fusion fail under both experimental conditions.

(C and D) To confirm the requirement for dynein, we assayed the ability of micromanipulated spindles to fuse following assembly in immunodepleted extracts containing less than 2.5% of the endogenous protein ([C]; see Supplemental Data and Figure S2). In these assays, pairs of bipolar microtubule arrays, which lacked focused poles as expected, were positioned initially with their long axes parallel to one another and with overlapped birefringence. All perturbations of cytoplasmic dynein function completely blocked spindle fusion. In contrast, spindles assembled in XCTK2-depleted extracts still fused (D). Scale bars represent 25 μm.

problematic with Eg5-inhibited monopoles (see Supplemental Data). In summary, the results of the monopole fusion experiments are consistent with the hypothesis that pulling forces are generated by a mechanism involving dynein motor activity and associated crosslinking to slide and pull together oppositely oriented polar microtubules.

Based on this hypothesis, we made two predictions, the first about dynein localization and the second about microtubule movements resulting from dynein-dependent crosslinking. In regards to localization, our monopole fusion experiments predicted that the motor should be present near the periphery of monopolar arrays, not simply at their poles. Indeed, this is the case. Although the labeling is weak relative to kinetochores and the pole, dynein does colocalize with tubulin throughout the structure (Figure 5E). To address microtubule movement resulting from antiparallel microtubule interactions, we added a low level (125 nM) of fluorescently labeled EB-1 to assembled monopoles (as in Figure 5D) and viewed monopole fusion with high-resolution confocal microscopy (Figure 5F) [26]. As EB-1 tracks only the plus ends of growing microtubules, our analysis was limited to this subpopulation of microtubules. We reasoned that pulling forces generated at intersection points lying off of the interpolar axis would result in movement of the interacting microtubules toward the axis. In individual monopoles, the tracks of EB1 comets generally radiate outward from a single point (Figure 5D and Movie S11), but, during the initial stages of monopole fusion, we observed EB1 comet trajectories with transverse movements toward the interpolar axis (Figures 5F and 5G and Movie S12). Importantly, this "clustering" of microtubules indicates that forces generated at distal sites along the microtubules are transmitted to the rest of the microtubule array. Furthermore, this bundling occurred in a region away from chromosomes and associated kinetochores, thus excluding involvement of kinetochore-associated dynein [27] or parallel sliding of kinetochore-nucleated microtubules [28].

## Discussion

The defined orientation of microtubules within monopolar arrays [12, 24, 29] and the sensitivity of fusion to dynein perturbation (Figure 5B) allow us to postulate that the microtubule-microtubule interactions responsible for fusion occur between oppositely oriented microtubules and are mediated by dynein. This represents an additional functional geometry for dynein motor complexes, which contrasts the prevailing view in the literature: that dynein-mediated focusing of microtubule minus ends into poles occurs largely via sliding and transport of microtubules of the same polarity [24, 30–32]. In this sliding model, dynein pulls the minus end of one microtubule toward the minus end of another, as originally proposed by Karsenti and colleagues to explain taxol aster formation in *Xenopus* egg extracts [33]. This parallel sliding is thought to be mediated by dynein-NuMA complexes localized at or near microtubule minus ends [24, 34]. Our immunofluorescence data show that dynein localizes throughout monopolar microtubule arrays, even toward the more distal aspects of the array near presumptive microtubule plus ends (Figure 5E). It is possible that minus ends are distributed throughout the monopole as well [19, 20], and because this distribution is not known, our experiments do not resolve clearly where (or how) dynein complexes are bound along the microtubules they slide. However, dynein has been show to localize to growing plus ends [35–37], presumably to better position the motor to capture its intended targets. It is possible that these dynein-dependent forces are somehow coupled to plus end polymerization dynamics, perhaps explaining why taxol-induced asters in *Xenopus* egg extracts do not fuse and instead form tessellated patterns in the plane of the coverslip surface (T.J.M., unpublished data). Alternatively, dynein complexes capable of crosslinking microtubules might bind all along the walls of existing microtubules by using unknown accessory proteins other than NuMA. Future analyses are needed to characterize the nature of this binding, which is critically important in understanding how this sliding filament mechanism might contribute to spindle assembly and length maintenance [38, 39].

Based on our data, we propose a model whereby the primary mechanism driving spindle fusion is dynein-dependent pulling forces between overlapping polar microtubule arrays that extend radially from focused poles. These forces alone can readily explain both monopole fusion and the jackknifing mode of bipole fusion (Figure 6). For monopoles, dynein crosslinks oppositely oriented microtubules from both arrays, generating a tensile force that pulls the poles together. Because Eg5 is inhibited, the poles slide together and ultimately merge. During jackknifing, wherein the axis of

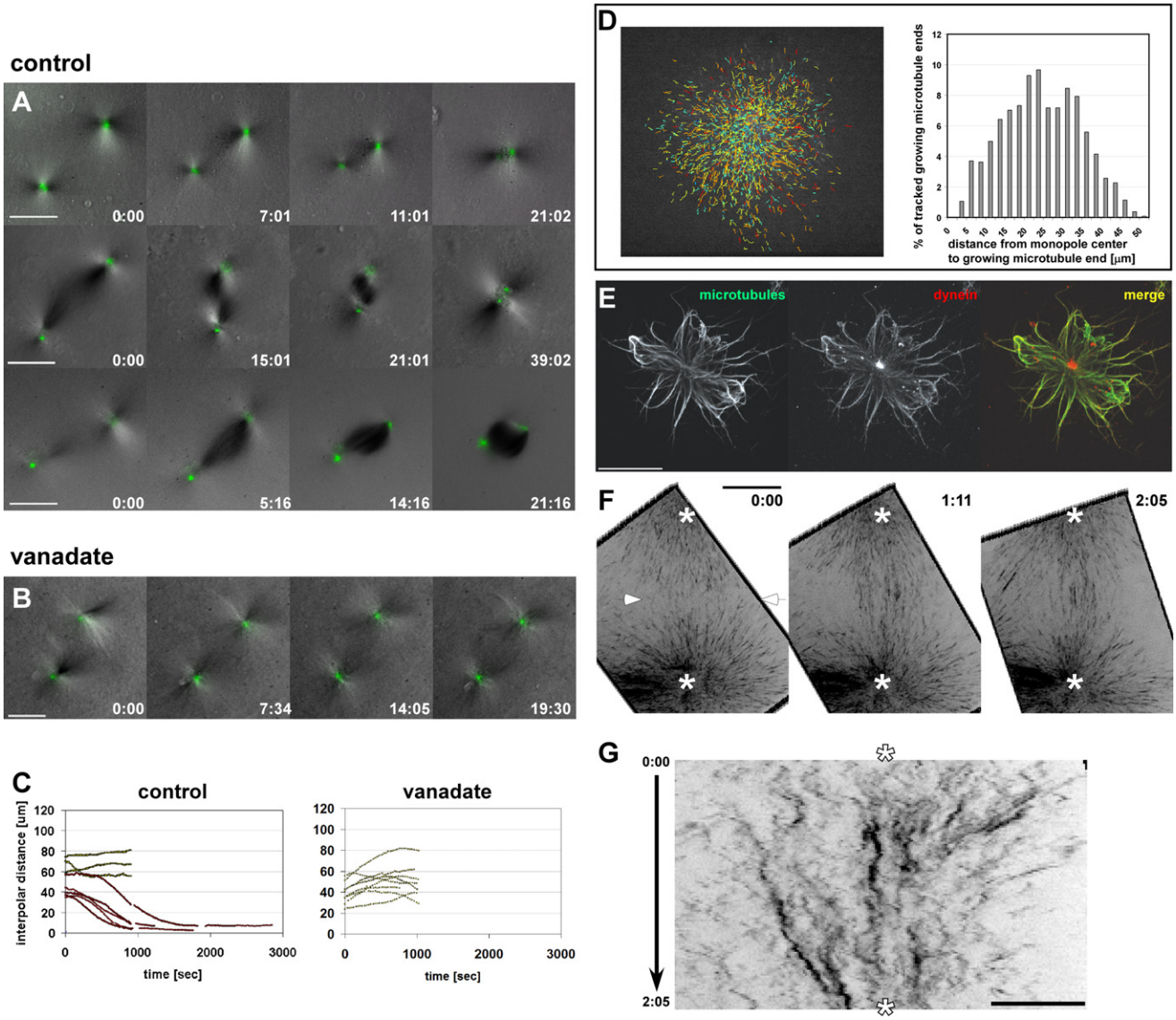


Figure 5. The Fusion of Eg5-Inhibited Monopoles is Mediated by Dynein-Dependent Sliding of Antiparallel Microtubules

Following spindle assembly, *Xenopus* egg extracts were treated with the Eg5-specific inhibitors STLC (25 μM) or monastrol (100 μM). Poles were labeled with anti-NuMA antibodies conjugated to AlexaFluor 488 to facilitate automated pole tracking. Fusion was monitored with polarization optics and fluorescence microscopy.

(A) Three examples of Eg5-inhibited monopole fusion demonstrating varying degrees of increased interpolar birefringence observed during fusion (total n > 20 pairs).

(B and C) The addition of 25 μM vanadate (~5–~10 min prior to imaging) inhibited monaster fusion. For each experimental condition, the interpolar distance between anti-NuMA-labeled poles was plotted as a function of time (C). In these plots, the initial separations between monopole pairs are equal to the interpolar distance values at time t = 0.

(D) Growing microtubule plus ends were visualized by addition of 125 nM AlexaFluor 488-labeled EB1 and recorded with confocal microscopy. The image is a single frame selected from an ~2 min time lapse recording overlayed with EB1 tracks (n = 1396 tracks with a minimum lifetime of four consecutive frames). The histogram shows the distribution of radial distances from the monopole center (see Experimental Procedures) to the distal end of each EB1 track.

(E–G) In (E), Eg5-inhibited monopoles were spun down on coverslips following fixation as described in [48]. The monopoles were then processed for immunofluorescence microscopy by using antibodies against tubulin (green) and the 70.1/74 kDa intermediate chain of dynein (red). The extent and dynamics of microtubule plus ends during monopole fusion were assessed by labeling growing microtubule ends by adding 125 nM GFP-EB1 to assembled monopoles ([F] and [G]; see Movie S2). The images in (F) (shown in inverted contrast) are from a time-lapse series of two monopoles, marked by asterisks, at the initial stages of interaction (a third monopole is out of the field toward the lower right). Microtubule density increases in a region half-way between the poles. In (G), a kymograph of the linear region between the two arrowheads in (F) is used to show movements of EB1-labeled ends toward the interpolar axis (asterisks mark the approximate position of the poles). All scale bars represent a length of 25 μm, except for the scale bar in (G), which is equivalent to 10 μm.

one spindle is initially perpendicular to the other, the same forces pull the closest two poles together first, likely because the shorter distance stochastically favors higher peripheral microtubule density and a larger number of force-generating interactions between overlapped peripheral microtubule arrays. At the same time, the spindle rotates in the direction

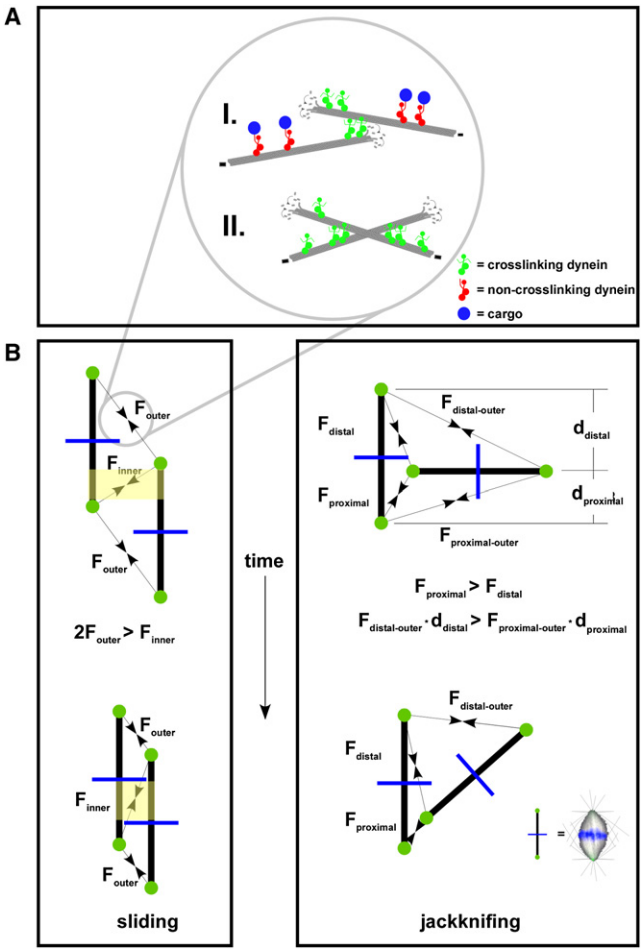


Figure 6. A Model for Bipolar Spindle Fusion

(A) A cartoon schematic showing ways in which dynein-dependent sliding of antiparallel, peripheral microtubules might occur. These two models differ in that the first relies on plus end growth to license the dynein motor, permitting crosslinking only near growing plus ends. In the second, dynein crosslinking is independent of plus end growth and can occur anywhere along the length of the microtubule.

(B) Dynein-dependent sliding of oppositely oriented, peripheral microtubules extending from each pole can account for both modes of bipolar spindle merging. For the sliding mode, we predict that the sum of forces generated between the outer pole of one spindle and inner pole of the other is greater than the attractive force between the two inner poles. Eg5-dependent sliding in regions of antiparallel overlap between spindle microtubules (highlighted in yellow) might antagonize the dynein-mediated pulling forces, contributing to proximal pole separation. The jackknifing mode is more complex because it requires the generation of torque. In each of our T-bone experiments, the two nearest poles moved together first, likely due to $F_{proximal}$ being greater than $F_{distal}$. However, this imbalance would not be expected to generate the torque required for the observed jackknifing. We propose that the initial geometry creates a mechanical advantage (i.e., longer lever arm) for $F_{distal\text{-}outer}$, thereby generating a torque that favors a rotation in the counterclockwise direction as drawn.

dictated by the highest torque, which is generated by dynein-dependent pulling forces between the overlapped peripheral microtubule arrays from the distal poles.

If pole-pole attraction is the dominant mechanism responsible for fusion, it seems somewhat paradoxical that the proximal poles slide away from each other when spindles are positioned with their axes parallel and poles overlapped (i.e., during spindle sliding) (Figure 1). This can be explained, however, provided that the overlapped geometry allows for pulling forces to be generated between the proximal pole of each spindle and the distal pole of the other (see "$F_{OUTER}$" in Figure 6B) and that these forces, in sum, are greater than the pulling force between the two proximal poles ("$F_{INNER}$" in Figure 6B). Alternatively, spindle sliding may occur because kinesin-5 (Eg5) is concentrated on spindle microtubules near the poles [40, 41], with its plus end-directed motility acting to antagonize dynein minus end-directed motility, significantly reducing the net pulling force between the proximal poles. Although this latter explanation is plausible, we favor the former mechanism because bipolar spindle sliding did not occur when dynein alone was inhibited (see Figure 4).

The same forces responsible for pair-wise bipole and monopole fusion might also be at work within a single bipolar spindle, affecting steady-state spindle length by antagonizing Eg5 sliding. Indeed, the observation that Eg5 and dynein antagonize one another to regulate *Xenopus* extract spindle length is consistent with this idea [15, 19]. Furthermore, our observation that bipolar spindle sliding occurs at a velocity that is slower than that observed in vitro for unloaded dynein ($\sim$75 $\mu m min^{-1}$) [42] or dynein-dependent sliding of parallel microtubules in the spindle ($\sim$6 $\mu m min^{-1}$) [18] might be a result of this antagonism; however, it could also be due to the effects of molecular friction and viscous drag (although the drag forces at the sliding speeds observed are likely to be negligible). Interestingly, monopole fusion occurred at a faster rate than bipole sliding, 2.8 $\pm$ 0.8 $\mu m min^{-1}$ and 1.2 $\pm$ 0.4 $\mu m min^{-1}$, respectively ($p \ll 0.05$). It is also possible that interactions between peripheral microtubules and those within the spindle are regulated differently due to spatial and/or geometric parameters. This could explain why dynein forces seem to dominate antiparallel interactions between peripheral microtubules during bipolar spindle fusion (where both motors are active), whereas those forces generated by Eg5 dominate within the spindle, particularly near the midzone, as evident by persistent microtubule flux. Indeed, spatial variations of Eg5 dynamics within the spindle have been characterized [40, 41]. Consistent with this idea, the motor's activity has been shown to be positively affected by RanGTP and its downstream effectors [43], which form a gradient around chromosomes at the metaphase plate [44]. Alternatively, the oblique angles made by intersecting peripheral microtubules might favor force generation by a given motor type over another.

Independent of the molecular mechanisms, spindle fusion demonstrates the remarkable architectural plasticity of the spindle and provides unique insight into how this property might be governed. That the postfusion spindle is approximately the same size as its predecessors demonstrates that steady-state spindle size is only modestly affected by a doubling of the chromosomal number, an observation that is consistent with others in the literature [21, 45]. The fact that spindles maintain some sense of their own structural identity during pair-wise fusion, with aligned chromosomes and focused poles, suggests a constancy of form unaffected by predicted changes in the shape of putative signaling gradients localized around chromosomes, at least over the time scale of fusion. This adds credence to the idea that, once assembled and organized, the microtubules of the spindle themselves provide structural "feedback" that helps to maintain spindle shape, possibly due to microtubule-dependent nucleation of microtubules within the spindle [46].

## Experimental Procedures

### Reagents

All reagents, unless stated otherwise, were purchased from Sigma-Aldrich and are of the highest quality available.

### Spindle Assembly in *X. laevis* Egg Extracts

CSF-arrested egg extracts were prepared as described by Murray and colleagues [47, 48]. "Cycled" spindles, prepared as described in [48], were allowed to assemble for 1–1.5 hr at 18°C before experimentation. Monopolar spindles were assembled in the presence of STLC (25 uM) or monastrol (100 uM), both small molecule inhibitors of Eg5. A comparison of monopoles in each condition revealed no discernable differences in architecture or behavior during fusion experiments.

### Spindle Micromanipulation and Imaging

To prepare micromanipulation chambers, 22 $mm^2$ coverslips were used to cover circular cutouts (~3/4" diameter) in custom-made metal slides (3" × 1" × 1/32"). The #1.5 coverslip (Fisher Scientific) was adhered to a preheated slide with melted VALAP (1:1:1 vasoline, lanolin, and paraffin) applied around the cutout. The metal slide was allowed to cool, and a small aliquot (~5–7 μl) of extract was spread over the glass surface with a pipette tip and overlayed with paraffin oil (300 μl) to prevent the sample from drying out during subsequent imaging.

Micromanipulation experiments were conducted with a TE2000e inverted microscope stand (Nikon) equipped with a motorized microscope stage (Applied Scientific Instrumentation). Dual pneumatic micromanipulators (Narishige) were mounted directly to the condenser arm of the microscope and adjusted so that the opposing needles entered the well at shallow angles to the coverslip surface. The borosilicate glass needles used for micromanipulation were made with a model P-97 micropipette puller (Sutter Instrument Company). The needles had long, tapered ends (~9 mm from the base of the taper to the needle tip) and were lowered through the paraffin oil overlay and into the extract for manipulation. Polarization optics (i.e., a crossed polarizer and analyzer) in combination with a 20× differential interference contrast (DIC) objective (Nikon Plan Fluor, 20×/0.75 NA MImm) were used to visualize spindles during micromanipulation. The needles were readily visible under these imaging conditions. Images were acquired with a cooled CCD camera (Orca-ER; Hamamatsu) or a cooled EM-CCD camera (iXon; Andor).

For real-time imaging during spindle fusion, we used the multimode data acquisition feature of Metamorph software (Molecular Devices) to control image acquisition. The positions of poles were tracked with either the "track object" or "track points" applications in Metamorph. Where needed, rotation of acquired image stacks was performed with custom MATLAB software (The MathWorks) written by J.C. Gatlin. Unless otherwise stated, at least three different extracts were used for each experimental condition.

Various fluorescently labeled antibodies and proteins were used to see specific spindle elements during real-time imaging of spindle fusion. To visualize spindle poles for fusion velocity measurements, Alexa Fluor-488-labeled (Invitrogen) anti-NuMA antibody [49] was added to extracts (final concentration of 10 $\mu g ml^{-1}$) before spindle assembly. Growing plus ends were marked by recombinant EB1 (125 nM) directly labeled with the same dye and added to extracts prior to imaging [26]. Peripheral microtubules were labeled by the incorporation of Alexa Fluor 647-tubulin (~100 $ng ml^{-1}$) added to assembled spindles. DAPI (1 $\mu g ml^{-1}$) was also added to some extracts to view chromosomes during fusion. High-resolution digital images were collected with a cooled CCD Orca ER or cooled EM-CCD Andor iXon camera coupled to a Yokogawa spinning disk confocal unit (CSU10, PerkinElmer) mounted on a TE300 inverted microscope (Nikon). A 60× Plan Apochromat, 1.4 NA DIC objective was used for all high-resolution imaging. The system was controlled with Metamorph software.

Samples were prepared for indirect immunofluorescence as described previously [48] with only minor changes. Briefly, assembled monopoles were fixed with paraformaldehyde, pelleted onto coverslips, and then post-fixed in −20°C methanol. Following rehydration in PHEM + 0.1% Triton X-100 (TX), the coverslips were blocked in PHEM + 5% boiled donkey serum for 30 min to 1 hr. Samples were then incubated in blocking buffer with primary antibodies against α-tubulin (rat polyclonal, Serotec) and 70–74 kD intermediate chain of cytoplasmic dynein ([50], a generous gift from K. Vaughan). After three rinses in blocking buffer, samples were incubated for 1 hr in blocking buffer with fluorophore-conjugated secondary antibodies (Invitrogen), rinsed three times in PHEM-TX, mounted on slides in mounting buffer (20 mM Tris [pH 8.0], 0.5% N-propyl gallate, and 90% Glycerol), and sealed with nail polish.

### Immunodepletions and Dynein Perturbation

To immunodeplete proteins from egg extracts, we first bound antibodies to protein-A-conjugated magnetic beads (Invitrogen). A 300 μl volume of bead suspension was rinsed three times in *Xenopus* buffer (XB; 10 mM K-HEPES [pH 7.7], 100 mM KCl, 1 mM $MgCl_2$, 0.1 mM $CaCl_2$, and 50 mM sucrose). For each immunodepletion, 90 μg of antibody was added to the equivalent of 300 ul of the original bead suspension and allowed to conjugate overnight with end-over-end rotation at 4°C. Antibody-conjugated beads were rinsed three times and resuspended in 300 μl XB. Beads from 100 μl of this suspension were resuspended in 150 μl of CSF-arrested extract and incubated for 1 hr on ice with occasional gentle agitation. The beads were collected on ice for 10 min to facilitate complete retrieval from the viscous extract. The remaining partially depleted extract was then used to resuspend a new 100 μl aliquot of antibody-conjugated beads, and the process was repeated for a total of three immunodepletions. Cycled spindle assembly reactions were carried out in the immunodepleted extracts as described above. The antibodies used for these experiments were a monoclonal antibody anti-74 kD dynein intermediate chain (IgG isotype; Chemicon) and a rabbit polyclonal anti-XCTK2 [22].

For dynein perturbation studies, vanadate (25 μM) was added to extracts from 100 mM stock. For antibody perturbation, concentrated anti-70.1 kD DIC antibody (Sigma Aldrich) was added to extracts containing preassembled spindles to 1 $mg ml^{-1}$ with a volume ratio of 1:10 [18]. Imaging of spindle fusion was typically started 5–10 min after the addition of either reagent.

### Determination of Monopole Size by EB1 Tracking

Individual EB1 spot features were identified and localized in all images with a scale-space theory-based three-step band-pass detection algorithm (A.M., unpublished data). Feature tracking was accomplished by single-particle tracking as described in [51], wherein Kalman filtering was used to project particle paths for more robust particle association between frames. The center of the monopole was determined as the center of mass of the pair-wise intersections between the axes extrapolated from all Alexa Fluor 488-EB1 tracks present in a frame. To compensate for drift in the monopole spindle position over time, we updated the pole center coordinates in every time point of the movie and performed further analysis relative to this position. All programs for Alexa Fluor 488-EB1 feature analysis and graphical representation were written in the Danuser laboratory in MATLAB and C++.

### Statistical Analyses

All statistical analyses and graphing were done with Microsoft Excel software. Reported results are mean values ± SD.

### Supplemental Data

Supplemental Data include Supplemental Experimental Procedures, 3 figures, and 12 movies and can be found with this article online at http://www.current-biology.com/supplemental/S0960-9822(09)00627-7.

### Acknowledgments

We thank L. Cameron (Dana-Farber Cancer Institute), A. Joglekar (University of North Carolina at Chapel Hill), and S. Dumont (Harvard Medical School) for helpful discussions, comments, and critical reading of the manuscript, as well as other members of the Salmon Laboratory and the Cell Division Group. We also thank K. Vaughan (University of Notre Dame) for the generous gift of anti-dynein intermediate chain antibody. A special thanks goes to H. Luther and M. Peterson (Marine Biological Laboratories) for help with acquiring necessary equipment. This work was supported by National Institute of General Medicine grants to J.C.G. (F32GM080049), E.D.S. (GM24364), and G.D. (GM60678). T.J.M. was funded by the National Cancer Institute (CA078048-09).

Received: November 13, 2008
Revised: January 3, 2009
Accepted: January 7, 2009
Published online: February 19, 2009

**References**

1. Walczak, C.E., and Heald, R. (2008). Mechanisms of mitotic spindle assembly and function. Int. Rev. Cytol. *265*, 111–158.
2. O'Connell, C.B., and Khodjakov, A.L. (2007). Cooperative mechanisms of mitotic spindle formation. J. Cell Sci. *120*, 1717–1722.
3. Savoian, M.S., and Rieder, C.L. (2002). Mitosis in primary cultures of Drosophila melanogaster larval neuroblasts. J. Cell Sci. *115*, 3061–3072.
4. Church, K., Nicklas, R.B., and Lin, H.P. (1986). Micromanipulated bivalents can trigger mini-spindle formation in Drosophila melanogaster spermatocyte cytoplasm. J. Cell Biol. *103*, 2765–2773.
5. Maiato, H., Rieder, C.L., and Khodjakov, A. (2004). Kinetochore-driven formation of kinetochore fibers contributes to spindle assembly during animal mitosis. J. Cell Biol. *167*, 831–840.
6. Tulu, U.S., Fagerstrom, C., Ferenz, N.P., and Wadsworth, P. (2006). Molecular requirements for kinetochore-associated microtubule formation in mammalian cells. Curr. Biol. *16*, 536–541.
7. Torosantucci, L., De Luca, M., Guarguaglini, G., Lavia, P., and Degrassi, F. (2008). Localized RanGTP accumulation promotes microtubule nucleation at kinetochores in somatic mammalian cells. Mol. Biol. Cell *19*, 1873–1882.
8. Sharp, D.J., Yu, K.R., Sisson, J.C., Sullivan, W., and Scholey, J.M. (1999). Antagonistic microtubule-sliding motors position mitotic centrosomes in Drosophila early embryos. Nat. Cell Biol. *1*, 51–54.
9. Kapitein, L.C., Peterman, E.J., Kwok, B.H., Kim, J.H., Kapoor, T.M., and Schmidt, C.F. (2005). The bipolar mitotic kinesin Eg5 moves on both microtubules that it crosslinks. Nature *435*, 114–118.
10. Miyamoto, D.T., Perlman, Z.E., Burbank, K.S., Groen, A.C., and Mitchison, T.J. (2004). The kinesin Eg5 drives poleward microtubule flux in Xenopus laevis egg extract spindles. J. Cell Biol. *167*, 813–818.
11. Shirasu-Hiza, M., Perlman, Z.E., Wittmann, T., Karsenti, E., and Mitchison, T.J. (2004). Eg5 causes elongation of meiotic spindles when flux-associated microtubule depolymerization is blocked. Curr. Biol. *14*, 1941–1945.
12. Mitchison, T.J., Maddox, P., Groen, A., Cameron, L., Perlman, Z., Ohi, R., Desai, A., Salmon, E.D., and Kapoor, T.M. (2004). Bipolarization and poleward flux correlate during Xenopus extract spindle assembly. Mol. Biol. Cell *15*, 5603–5615.
13. Ross, J.L., Wallace, K., Shuman, H., Goldman, Y.E., and Holzbaur, E.L. (2006). Processive bidirectional motion of dynein-dynactin complexes in vitro. Nat. Cell Biol. *8*, 562–570.
14. Mayer, T.U., Kapoor, T.M., Haggarty, S.J., King, R.W., Schreiber, S.L., and Mitchison, T.J. (1999). Small molecule inhibitor of mitotic spindle bipolarity identified in a phenotype-based screen. Science *286*, 971–974.
15. Mitchison, T.J., Maddox, P., Gaetz, J., Groen, A., Shirasu, M., Desai, A., Salmon, E.D., and Kapoor, T.M. (2005). Roles of polymerization dynamics, opposed motors, and a tensile element in governing the length of Xenopus extract meiotic spindles. Mol. Biol. Cell *16*, 3064–3076.
16. Yang, G., Houghtaling, B.R., Gaetz, J., Liu, J.Z., Danuser, G., and Kapoor, T.M. (2007). Architectural dynamics of the meiotic spindle revealed by single-fluorophore imaging. Nat. Cell Biol. *9*, 1233–1242.
17. Gaetz, J., and Kapoor, T.M. (2004). Dynein/dynactin regulate metaphase spindle length by targeting depolymerizing activities to spindle poles. J. Cell Biol. *166*, 465–471.
18. Heald, R., Tournebize, R., Blank, T., Sandaltzopoulos, R., Becker, P., Hyman, A., and Karsenti, E. (1996). Self-organization of microtubules into bipolar spindles around artificial chromosomes in Xenopus egg extracts. Nature *382*, 420–425.
19. Burbank, K.S., Mitchison, T.J., and Fisher, D.S. (2007). Slide-and-cluster models for spindle assembly. Curr. Biol. *17*, 1373–1383.
20. Burbank, K.S., Groen, A.C., Perlman, Z.E., Fisher, D.S., and Mitchison, T.J. (2006). A new method reveals microtubule minus ends throughout the meiotic spindle. J. Cell Biol. *175*, 369–375.
21. Brown, K.S., Blower, M.D., Maresca, T.J., Grammer, T.C., Harland, R.M., and Heald, R. (2007). Xenopus tropicalis egg extracts provide insight into scaling of the mitotic spindle. J. Cell Biol. *176*, 765–770.
22. Walczak, C.E., Verma, S., and Mitchison, T.J. (1997). XCTK2: A kinesin-related protein that promotes mitotic spindle assembly in Xenopus laevis egg extracts. J. Cell Biol. *136*, 859–870.
23. Shimizu, T., Toyoshima, Y.Y., Edamatsu, M., and Vale, R.D. (1995). Comparison of the motile and enzymatic properties of two microtubule minus-end-directed motors, ncd and cytoplasmic dynein. Biochemistry *34*, 1575–1582.
24. Heald, R., Tournebize, R., Habermann, A., Karsenti, E., and Hyman, A. (1997). Spindle assembly in Xenopus egg extracts: Respective roles of centrosomes and microtubule self-organization. J. Cell Biol. *138*, 615–628.
25. Groen, A.C., Needleman, D., Brangwynne, C., Gradinaru, C., Fowler, B., Mazitschek, R., and Mitchison, T.J. (2008). A novel small-molecule inhibitor reveals a possible role of kinesin-5 in anastral spindle-pole assembly. J. Cell Sci. *121*, 2293–2300.
26. Tirnauer, J.S., Grego, S., Salmon, E.D., and Mitchison, T.J. (2002). EB1-microtubule interactions in Xenopus egg extracts: Role of EB1 in microtubule stabilization and mechanisms of targeting to microtubules. Mol. Biol. Cell *13*, 3614–3626.
27. Pfarr, C.M., Coue, M., Grissom, P.M., Hays, T.S., Porter, M.E., and McIntosh, J.R. (1990). Cytoplasmic dynein is localized to kinetochores during mitosis. Nature *345*, 263–265.
28. Khodjakov, A., Copenagle, L., Gordon, M.B., Compton, D.A., and Kapoor, T.M. (2003). Minus-end capture of preformed kinetochore fibers contributes to spindle morphogenesis. J. Cell Biol. *160*, 671–683.
29. Kapoor, T.M., Mayer, T.U., Coughlin, M.L., and Mitchison, T.J. (2000). Probing spindle assembly mechanisms with monastrol, a small molecule inhibitor of the mitotic kinesin, Eg5. J. Cell Biol. *150*, 975–988.
30. Tulu, U.S., Rusan, N.M., and Wadsworth, P. (2003). Peripheral, non-centrosome-associated microtubules contribute to spindle formation in centrosome-containing cells. Curr. Biol. *13*, 1894–1899.
31. Gaetz, J., Gueroui, Z., Libchaber, A., and Kapoor, T.M. (2006). Examining how the spatial organization of chromatin signals influences metaphase spindle assembly. Nat. Cell Biol. *8*, 924–932.
32. Chakravarty, A., Howard, L., and Compton, D.A. (2004). A mechanistic model for the organization of microtubule asters by motor and non-motor proteins in a mammalian mitotic extract. Mol. Biol. Cell *15*, 2116–2132.
33. Verde, F., Berrez, J.M., Antony, C., and Karsenti, E. (1991). Taxol-induced microtubule asters in mitotic extracts of Xenopus eggs: Requirement for phosphorylated factors and cytoplasmic dynein. J. Cell Biol. *112*, 1177–1187.
34. Merdes, A., Heald, R., Samejima, K., Earnshaw, W.C., and Cleveland, D.W. (2000). Formation of spindle poles by dynein/dynactin-dependent transport of NuMA. J. Cell Biol. *149*, 851–862.
35. Vaughan, K.T., Tynan, S.H., Faulkner, N.E., Echeverri, C.J., and Vallee, R.B. (1999). Colocalization of cytoplasmic dynein with dynactin and CLIP-170 at microtubule distal ends. J. Cell Sci. *112*, 1437–1447.
36. Lee, W.L., Oberle, J.R., and Cooper, J.A. (2003). The role of the lissencephaly protein Pac1 during nuclear migration in budding yeast. J. Cell Biol. *160*, 355–364.
37. Han, G., Liu, B., Zhang, J., Zuo, W., Morris, N.R., and Xiang, X. (2001). The Aspergillus cytoplasmic dynein heavy chain and NUDF localize to microtubule ends and affect microtubule dynamics. Curr. Biol. *11*, 719–724.
38. Mcintosh, J.R., Hepler, P.K., and Van Wie, D.G. (1969). Model for Mitosis. Nature *224*, 659–663.
39. Nedelec, F. (2002). Computer simulations reveal motor properties generating stable antiparallel microtubule interactions. J. Cell Biol. *158*, 1005–1015.
40. Kapoor, T.M., and Mitchison, T.J. (2001). Eg5 is static in bipolar spindles relative to tubulin: Evidence for a static spindle matrix. J. Cell Biol. *154*, 1125–1133.
41. Uteng, M., Hentrich, C., Miura, K., Bieling, P., and Surrey, T. (2008). Poleward transport of Eg5 by dynein-dynactin in Xenopus laevis egg extract spindles. J. Cell Biol. *182*, 715–726.
42. Paschal, B.M., and Vallee, R.B. (1987). Retrograde transport by the microtubule-associated protein MAP 1C. Nature *330*, 181–183.
43. Wilde, A., Lizarraga, S.B., Zhang, L., Wiese, C., Gliksman, N.R., Walczak, C.E., and Zheng, Y. (2001). Ran stimulates spindle assembly by altering microtubule dynamics and the balance of motor activities. Nat. Cell Biol. *3*, 221–227.
44. Kalab, P., Pralle, A., Isacoff, E.Y., Heald, R., and Weis, K. (2006). Analysis of a RanGTP-regulated gradient in mitotic somatic cells. Nature *440*, 697–701.
45. Wuhr, M., Chen, Y., Dumont, S., Groen, A.C., Needleman, D.J., Salic, A., and Mitchison, T.J. (2008). Evidence for an upper limit to mitotic spindle length. Curr. Biol. *18*, 1256–1261.

46. Mahoney, N.M., Goshima, G., Douglass, A.D., and Vale, R.D. (2006). Making microtubules and mitotic spindles in cells without functional centrosomes. Curr. Biol. *16*, 564–569.
47. Murray, A.W. (1991). Cell cycle extracts. Methods Cell Biol. *36*, 581–605.
48. Desai, A., Murray, A., Mitchison, T.J., and Walczak, C.E. (1999). The use of Xenopus egg extracts to study mitotic spindle assembly and function. Methods Cell Biol. *61*, 385–412.
49. Groen, A.C., Cameron, L.A., Coughlin, M., Miyamoto, D.T., Mitchison, T.J., and Ohi, R. (2004). XRHAMM functions in ran-dependent microtubule nucleation and pole formation during anastral spindle assembly. Curr. Biol. *14*, 1801–1811.
50. Vaughan, P.S., Leszyk, J.D., and Vaughan, K.T. (2001). Cytoplasmic dynein intermediate chain phosphorylation regulates binding to dynactin. J. Biol. Chem. *276*, 26171–26179.
51. Yang, G., Matov, A., and Danuser, G. (2005). Reliable tracking of large scale dense antiparallel particle motion for fluorescence live cell imaging. In 2005 IEEE Computer Society Conference on Computer Vision and Pattern Recognition, p. 138.